Numerical Analysis of Slow-Wave Instabilities in an Oversized Sinusoidally Corrugated Waveguide Driven by a Finitely Thick Annular Electron Beam

Kosuke OTUBO, Kazuo OGURA, Mitsuhisa YAMAKAWA and Yusuke TAKASHIMA

Graduate School of Science and Technology, Niigata University, 950-2181, Japan

(Received 8 January 2009 / Accepted 22 July 2009)

Three kinds of models are used for beam instability analyses: those based on a solid beam, an infinitesimally thin annular beam, and a finitely thick annular beam. In high-power experiments, the electron beam is an annulus of finite thickness. In this paper, a numerical code for a sinusoidally corrugated waveguide with a finitely thick annular beam is presented and compared with other models. Our analysis is based on a new version of the self-consistent linear theory that takes into account three-dimensional beam perturbations. Slow-wave instabilities in a K-band oversized sinusoidally corrugated waveguide are analyzed. The dependence of the Cherenkov and slow cyclotron instabilities on the annular thickness and guiding magnetic field are examined.

Keywords: annular beam, oversized sinusoidally corrugated waveguide, boundary condition, Cherenkov instability, slow cyclotron instability

DOI: 10.1585/pfr.5.S1047

1. Introduction

Backward wave oscillators (BWOs), which are high-power microwave sources, can be driven by an axially injected electron beam. In BWOs, periodically corrugated slow-wave structures (SWSs) are used to reduce the phase velocity of the electromagnetic mode close to the beam velocity. In many high-power experiments, cold cathodes are used, and the electron beam is a thin-walled annulus. To confine the electron beam, a guiding magnetic field is applied. In interactions between the beam and the electromagnetic waves, the cyclotron instability as well as the Cherenkov instability play an important role [1–3]. Near the cyclotron resonance or with a relatively low magnetic field, the beam motion perpendicular to the magnetic field cannot be ignored, and a more definitive study of BWOs that takes is into account vertical perturbation of the beam is required. A pioneering work for non-relativistic cases can be seen in Ref. [4], which considers the coupling between a sheet beam and a microwave circuit. New versions of the self-consistent relativistic field theory considering three-dimensional beam perturbations have been developed based on a solid beam [5, 6] and an infinitesimally thin annular beam [7]. For the latter, the sheet boundary is modulated due to the transverse modulation of the annular surface. Analyses of an infinitesimally thin annular beam need to be based on a different theory from those of thin-walled annular and solid beams. For a finitely thick annular beam, a numerical code has been developed and eigenmodes and slow-wave instabilities have been analysed in Ref. [8], in which a dielectric-loaded SWS is used for simplicity. The boundary condition at the beam's surface is different from that of the infinitesimally thin annular beam. The solid beam and finitely thick annular beam cases are based on the same beam boundary condition, but the number of the boundaries is different. An annular beam of finite thickness has outside and inside surfaces, and a solid beam has only an outside surface.

To increase the operating frequency and/or power-handling capability, oversized SWSs are successfully used. The diameter of an oversized SWS is larger than the free-space wavelength of the output electromagnetic waves by several times or more. Electromagnetic field properties are different from those in non-oversized cases, and the numerical code needs to be improved for oversized SWSs [9].

In this work, we develop a numerical code for a sinusoidally corrugated waveguide with a finitely thick annular beam and analyze slow-wave instabilities in an oversized sinusoidally corrugated waveguide. Our numerical code is based on the linear theory presented in Refs. [5, 6, 8]: non-linear effects are not included. Numerical parameters correspond to those in recent oversized BWO experiments designed for K-band operations in a weakly relativistic region at less than 100 kV [1–3]. The organization of this paper is as follows. In Sec. 2, we present a numerical method for an oversized SWS driven by a finitely thick annular beam. In the beam, eigenmodes due to three-dimensional perturbation are considered. In Sec. 3, numerical results are presented. The dependence of growth rate on the annular thickness and guiding magnetic field are examined. In Sec. 4, the conclusion of this paper is given.

author's e-mail: f06e072j@mail.cc.niigata-u.ac.jp

2. Numerical Method

We consider the periodically corrugated cylindrical waveguide shown in Fig. 1. The wall radius $R_w(z)$ varies along the axial direction z as $R_0 + h\cos(k_0 z)$, where the average radius $R_0 = 1.57\,\mathrm{cm}$, the corrugation amplitude $h = 0.17\,\mathrm{cm}$, the pitch length $z_0 = 0.34\,\mathrm{cm}$, and the corrugation wave number $k_0 = 2\pi/z_0$. A guiding magnetic field B_0 is applied uniformly in the axial direction. An electron beam propagates along the guiding magnetic field, and the electron beam is a finitely thick annulus. The beam is uniformly distributed from the inside radius R_{ba} to the outside radius R_{bb} with a beam thickness Δ_p ($= R_{\mathrm{bb}} - R_{\mathrm{ba}}$). The average radius of the electron beam is set to R_{a}. The regions outside and inside the beam are in a vacuum. The temporal and spatial phase factor of all perturbed quantities is assumed to be $\exp[\mathrm{i}(k_z z + m\theta - \omega t)]$. Here, m is the azimuthal mode number, and k_z is the axial wave number. Based on this model, the dispersion relation can be derived self-consistently considering the three-dimensional beam perturbations and boundary conditions. For the beam, relativistic effects are considered.

Since the SWS is spatially periodic with z_0, the fields in the SWS are expressed by the sum of a spatial harmonic series, the so-called Floquet series. The eigenfunctions for the cylindrical system are the Bessel functions, i.e., the mth-order Bessel functions of the first kind J_m and the second kind N_m. They have been used in the Floquet series for non-oversized BWO cases in which the electromagnetic modes are volumetric waves having a strong field near the axis.

For an the oversized BWO, the electromagnetic field is localized near the SWS wall, as shown in Fig. 2. Blue represents values less than 20 % of the maximum value of the electric field: green is 20 to 50 %, and the red is more than 50 %. All spatial harmonics are evanescent waves in the radial direction. If the spatial harmonics are expressed by J_m and N_m, they have extremely large imaginary parts This causes serious problems in numerical calculations. To avoid this difficulty, the expressions of spatial harmonics should be the mth-order modified Bessel functions of the first (I_m) and the second (K_m) kind. We improve the new self-consistent analysis by replacing the Bessel functions with the modified Bessel functions.

In the beam column (region II, $R_{\mathrm{a}} - \Delta_p/2 < r < R_{\mathrm{a}} + \Delta_p/2$), two eigenmodes exist. At zero beam velocity, these modes become the well-known O and X modes in a magnetized plasma for perpendicular propagation ($kz = 0$), and left and right circular waves for longitudinal propagation. In Ref. [5], two eigenmodes with $v \neq 0$ for arbitrary propagation are designated as the O and X modes. In this paper, the eigenmodes are composed of the Floquet series due to the spatial periodicity. The axial wave number of the p-th spatial harmonic is given by $kz + pk_0$ The corresponding vertical wave numbers are given by

$$k_{p\pm}^2 = \frac{-a_2 \pm \sqrt{a_2{}^2 - 4a_4 a_0}}{2a_4} \,. \tag{1}$$

Here,

$$a_4 = \omega''^2 - \frac{\omega_b^2}{\gamma^3}, \quad a_0 = \Delta\omega''^2\left(1 - \frac{\omega_b{}^2}{\gamma^3\omega'^2}\right)$$

$$a_2 = -\left[\left(\frac{\omega^2}{c^2} - k_p{}^2\right)\left(\omega''^2 - \frac{\omega_b{}^2}{\gamma^3}\right) - \frac{\omega_b{}^2}{\gamma c^2}\left(\omega'^2 - \frac{\omega_b{}^2}{\gamma^3}\right)\right]$$

$$- \left[\left(\frac{\omega^2}{c^2} - k_p{}^2\right)\omega''^2 - \frac{\omega_b{}^2}{\gamma c^2}\omega'^2\right]\left(1 - \frac{\omega_b{}^2}{\gamma^3\omega'^2}\right)$$

$$\Delta = \left(\frac{\omega^2}{c^2} - k_p{}^2 - \frac{\omega_b{}^2}{\gamma c^2}\frac{\omega'^2}{\omega''^2}\right)^2 - \left(\frac{\omega_b{}^2}{\gamma c^2}\frac{\omega'}{\omega''^2}\frac{\Omega}{\gamma}\right)^2 \tag{2}$$

and

$$\omega' = \omega - k_p v, \quad \omega''^2 = \left(\omega - k_p v\right)^2 - (\Omega/\gamma)^2 \,. \tag{3}$$

Here, γ is the relativistic factor, and ω_b and Ω are respectively the plasma frequency and non-relativistic cyclotron frequency of electrons, respectively. The vertical wave numbers k_{p+} and k_{p-} correspond to the + and − signs, respectively, in Eq. (1). As examined in Ref. [5], the O and X modes have k_{p+} and k_{p-} or k_{p-} and k_{p+}, respectively, depending on the parameters. Using the O and X modes, the

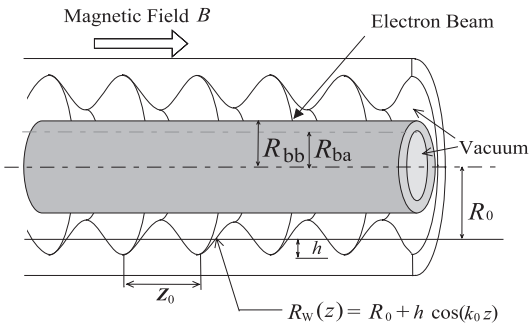

Fig. 1 Model for analysis. The cylindrical waveguide's wall is corrugated sinusoidally.

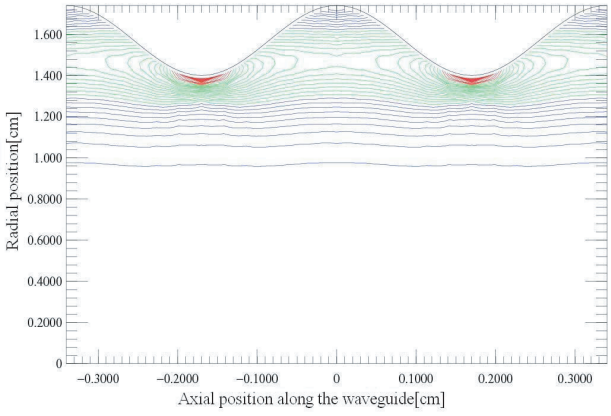

Fig. 2 Electric field distribution of TM_{01} mode in K-band SWS at $k_z z_0 = \pi$ (the π point).

axial components of the electromagnetic field in the beam are given by

$$E_{1z}^{II} = \sum_{p=-\infty}^{\infty} \left[D_p^+ I_m\left(k_{p+}r\right) + E_p^+ K_m\left(k_{p+}r\right) \right] + \sum_{p=-\infty}^{\infty} \left[D_p^- I_m\left(k_{p-}r\right) + E_p^- K_m\left(k_{p-}r\right) \right],$$

$$B_{1z}^{II} = \sum_{p=-\infty}^{\infty} \frac{i}{c} \left[F_p^+ I_m\left(k_{p+}r\right) + G_p^+ K_m\left(k_{p+}r\right) \right] + \sum_{p=-\infty}^{\infty} \frac{i}{c} \left[F_p^- I_m\left(x_{p-}r\right) + G_p^- K_m\left(k_{p-}r\right) \right]. \quad (4)$$

Four coefficients are necessary and sufficient for the expressions. The amplitudes F_p^+, G_p^+, F_p^- and G_p^- of B_{1z} are expressed by four coefficients, D_p^+, E_p^+, D_p^-, and E_p^-, of E_{1z} [5].

In the inner vacuum region of the annular column (region I, $r < R_a - \Delta_p/2$), the eigenmodes are the transverse magnetic (TM) and transverse electric (TE) modes. The axial components of the electric and magnetic wave are

$$E_{1z}^{I} = \sum_{p=-\infty}^{\infty} A_{Ep} I_m\left(x_p r\right),$$

$$B_{1z}^{I} = \sum_{p=-\infty}^{\infty} \frac{i}{c} A_{Bp} I_m\left(x_p r\right). \quad (5)$$

In the outer vacuum region of beam (region III, $r > R_a + \Delta_p/2$)

$$E_{1z}^{III} = \sum_{p=-\infty}^{\infty} \left[D_p^V I_m\left(x_p r\right) + E_p^V K_m\left(x_p r\right) \right],$$

$$B_{1z}^{III} = \sum_{p=-\infty}^{\infty} \frac{i}{c} \left[F_p^V I_m\left(x_p r\right) + G_p^V K_m\left(x_p r\right) \right]. \quad (6)$$

Here, A_{Ep}, A_{Bp}, D_p^V, E_p^V, F_p^V, and G_p^V are constants, and

$$x_p{}^2 = \frac{\omega^2}{c^2} - k_p{}^2 . \quad (7)$$

For bounded systems, Maxwell's equations should be solved subject to appropriate boundary conditions. The beam surfaces are modulated as the beam propagates. For a finitely thick annular beam, transverse modulation appears as an electric surface charge at the fixed boundary, as in Fig. 3.

At the beam surfaces ($r = R_a + \Delta_p/2$ and $r = R_a - \Delta_p/2$), we obtain the following four independent equations from the boundary conditions for the tangential components of the electric field, the axial component of the magnetic field, and the radial component of the electric flux density [5, 6].

$$E_{1z}^{va} - E_{1z}^{b} = 0,$$
$$E_{1\theta}^{va} - E_{1\theta}^{b} = 0,$$
$$B_{1z}^{va} - B_{1z}^{b} = 0,$$
$$\varepsilon_0 E_{1r}^{va} - (\varepsilon_0 E_{1r}^{b} + \sigma_1) = 0. \quad (8)$$

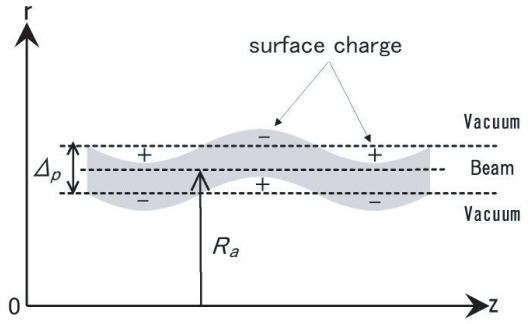

Fig. 3 Beam surface of finitely thick annular beam.

Here, σ_1 is the surface charge density at the beam surface. Superscripts "va" and "b" denote the vacuum side and beam side, respectively, on the surface. The boundary conditions correlate the coefficients of the field outside and inside the beam and are expressed by matrix forms as in Ref. [2], in which a dielectric-loaded SWS is used. In our periodic case, the conditions are formally expressed for each spatial harmonic as,

$$\begin{bmatrix} D_p^+ \\ E_p^+ \\ D_p^- \\ E_p^- \end{bmatrix} = \left[MX1\right] \cdot \begin{bmatrix} A_{Ep} \\ A_{Bp} \end{bmatrix}, \text{ for each } p, \text{ at } r = R_a - \Delta_p/2 . \quad (9)$$

$$\begin{bmatrix} D_p^V \\ E_p^V \\ F_p^V \\ G_p^V \end{bmatrix} = \left[MX2\right] \cdot \begin{bmatrix} D_p^+ \\ E_p^+ \\ D_p^- \\ E_p^- \end{bmatrix}, \text{ for each } p, \text{ at } r = R_a + \Delta_p/2 . \quad (10)$$

Here, $\left[MX1\right]$ is a 4×2 matrix, and $\left[MX2\right]$ is a 4×4 matrix: they are obtained from the boundary conditions after lengthy manipulation with the help of Mathematica. Using Eqs. (9) and (10), D_p^V, E_p^V, F_p^V, and G_p^V can be derived from two coefficients, A_{Ep} and A_{Bp}, as

$$\begin{bmatrix} D_p^V \\ E_p^V \\ F_p^V \\ G_p^V \end{bmatrix} = \left[MX2\right] \cdot \left[MX1\right] \cdot \begin{bmatrix} A_{Ep} \\ A_{Bp} \end{bmatrix}. \quad (11)$$

At the SWS wall ($r = R_w$), the two electric field components tangential to the wall (E_{1t} in the $r - z$ plane and $E_{1\theta}$ in the θ direction) should be zero,

$$E_{1z}(r = R_w) = 0 \text{ and } E_{1\theta}(r = R_w) = 0 . \quad (12)$$

From the spatial Fourier transform of Eq. (12), the dispersion equation can be derived. The dispersion equation has been derived in the previous works using this method [6,9]. The boundary conditions of Eq. (12) are reduced to the fol-

lowing relationship between A_{Ep} and A_{Bp},

$$\begin{bmatrix} D_{11} & D_{12} \\ D_{21} & D_{22} \end{bmatrix} \cdot \begin{bmatrix} \mathbf{A}_+ \\ \mathbf{A}_- \end{bmatrix} = 0 \,. \tag{13}$$

Here, D_{11}, D_{12}, D_{21}, and D_{22} are matrices of an infinite rank, and $\mathbf{A}_+$ and $\mathbf{A}_-$ are column vectors with elements A_{Ep} and A_{Bp}. The dispersion relation is obtained from the condition that Eq. (13) has a nontrivial solution and is given by

$$\det \begin{bmatrix} D_{11} & D_{12} \\ D_{21} & D_{22} \end{bmatrix} = 0 \,. \tag{14}$$

In our calculation, the rank of the matrix is truncated, i.e., the Floquet and Fourier harmonics numbers are limited to seven for each D_{ij} matrix.

From the two beam surfaces of an annular beam, eight equations are obtained. We reduce the number of equations from eight to four, as in Eq. (11), by eliminating four coefficients: D_p^+, E_p^+, D_p^-, and E_p^-. In Refs. [10,11], this kind of reduction is not performed, and these four coefficients must be derived numerically. This means that the matrix size corresponding to Eq. (13) increases by at least two times for our case. For periodic systems, a large matrix size is inevitable due to expantion of the Floquet and Fourier series. The increase in matrix size due to the boundaries causes serious numerical problems. It is very important to develop a numerical code while reducing the matrix size using the formulation of Eq. (11).

The method of this paper is based on the Rayleigh hypothesis, which assumes that the fields inside and outside the corrugation are expressed by the same Floquet series. To check the applicability of our numerical code, the field properties based on the Rayleigh hypothesis are compared with those obtained by direct numerical integration of Maxwell's equations using the higher-order implicit difference method (HIDM) [12]. The HIDM is free from the Rayleigh hypothesis. As is pointed out in Ref. [12], our self-consistent analysis is applicable to the oversized BWO.

3. Numerical Result

We analyzed the dispersion relation of an oversized sinusoidally corrugated waveguide driven by a finitely thick annular beam. In a system with a magnetized beam, such as that in Fig. 2, the electromagnetic modes are a hybrid of the TM and TE modes even in axisymmetric cases, due to the perturbed perpendicular to the magnetic field. The letters "EH" and "HE" are used to designate the hybrid mode. In this paper, TM is dominant in the EH mode, and TE is dominant in the HE mode.

Figure 4 shows the dispersion curves of the axisymmetric hybrid EH_{01} mode with a beam energy of 80 keV, current of 200 A, beam thickness of $\Delta p = 0.1$ cm, and B0 = 0.4 T. Four beam modes exist on the axially streaming beam. They are fast and slow space charge modes,

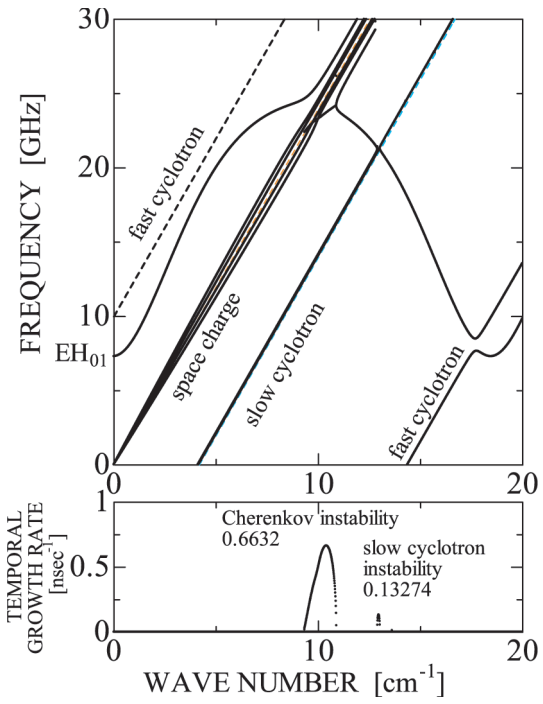

Fig. 4 Dispersion curves of axisymmetric mode ($m = 0$) with beam energy 80 keV, current 200 A, $R_{bb} = 1.35$ cm, $R_{ba} = 1.25$ cm and $B_0 = 0.4$ T.

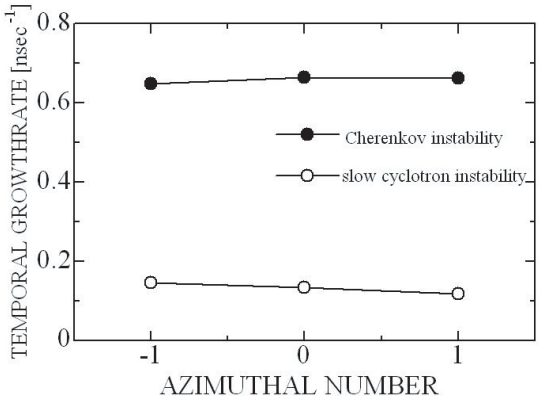

Fig. 5 Temporal growth rate of Cherenkov and slow cyclotron instabilities versus rotational direction of electromagnetic wave propagation.

fast and slow cyclotron modes. The slow space charge and slow cyclotron modes couple to the EH_{01} mode, resulting in the Cherenkov and slow cyclotron instabilities.

The growth rates of the slow cyclotron instability are plotted in Fig. 5 for $m = -1$, 0, and 1. The nonaxisymmetric instabilities are almost the same as the axisymmetric instability. Since the perturbation is assumed to be $\exp[i(k_z z + m\theta - \omega t)]$, electromagnetic waves propagate helically. The direction of rotation is rightward (leftward) in the laboratory frame of reference with positive (negative) m. For an oversized BWO, the growth rates are not affected by the rotational direction.

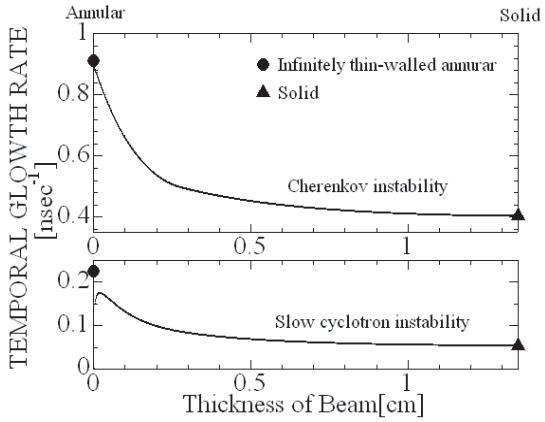

Fig. 6 Dependence of the temporal growth rate on beam thickness.

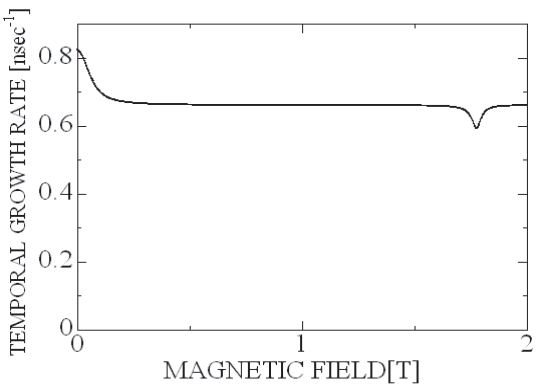

Fig. 7 Dependence of Cherenkov instability on B_0. Beam parameters are the same in Fig. 4.

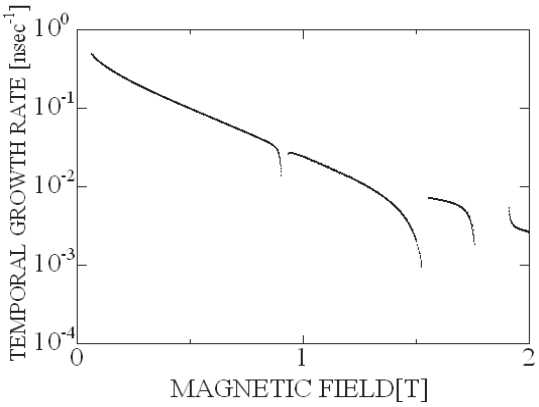

Fig. 8 Dependence of slow cyclotron instability on B_0. Beam parameters are the same in Fig. 4.

Figure 6 shows the dependence of the temporal growth rate on beam thickness Δ_p for the EH_{01} mode. The beam's outer radius is fixed at 1.35 cm, and the beam's inner radius has been changed with a fixed line density λ_0 and hence a fixed beam current. Here, we must distinguish λ_0 from the volume density n_0. In the case of a uniformly distributed beam, λ_0 is the product of the area of the beam's cross section and n_0. When Δ_p decreases, n_0 increases; this keeps λ_0 constant. The growth rate of the Cherenkov instability increases with a fixed beam current in the case of low Δ_p and large n_0. The growth rate of the slow cyclotron instability also increases with decreasing Δ_p and increasing n_0. However, in the region of $\Delta_p < 0.022$ cm, the growth rate decreases.

In the limit that the beam's inner radius is zero, the growth rate of the Cherenkov and slow cyclotron instabilities of a thin-walled annular beam approaches the growth rate of a solid beam, denoted by ▲ in Fig. 6. In the other limit that $\Delta_p \to 0$, the corresponding growth rates are those of an infinitesimally thin annular beam model and are denoted by (● in Fig. 6. Two models based on finite and zero Δ_p give almost the same results for the Cherenkov instability. For the slow cyclotron instability, the growth rates of the two models differ. This might be caused by the difference in the annulus: one has an internal structure between the inner and outer surfaces, and the other is just a sheet without any internal structure.

For the EH_{01} mode, the dependence of the temporal growth rate of the Cherenkov instability on the guiding magnetic field is shown in Fig. 7 and that of the slow cyclotron instability in Fig. 8. The growth rate of the Cherenkov instability hardly changes with variation in the magnetic field. However, in the region of $B_0 < 0.18$ T, the growth rate increases. In this region, the slow cyclotron instability merges into the Cherenkov instability. The dip in the growth rate in the vicinity of 1.8 T is attributed to resonant interaction of the space charge and fast cyclotron modes. Electromagnetic wave excitation by the space charge mode is suppressed by the fast cyclotron interaction. Such combined interaction is characteristic of a periodic SWS.

The growth rate of the slow cyclotron instability depend strongly on the magnetic field: it decreases with increasing magnetic field. The slow and fast cyclotron modes shift to the right and to the left, respectively, in Fig. 4. In the vicinity of 0.9 T and 1.8 T, the slow and fast cyclotron modes interact with each other, and the growth rate becomes discontinuous. At 1.5 T, the slow cyclotron mode begins to cross the EH_{01} mode at the 2π point with a very small growth rate at point 1 in Fig. 9. Other interaction points 2 and 3 appear in the forward region, as shown in Fig. 9. Note that the three points 1, 2, and 3 are on the same slow cyclotron mode. The dispersion curves of a periodic SWS are periodic in wave number space, and a one-period drawing has all the information we need. Figure 9 has a period of 18.5 cm^{-1}. The forward region from 18.5 cm^{-1} ($k_z z_0 = 2\pi$) to 27.7 cm^{-1} ($k_z z_0 = 3\pi/2$) can be seen in the forward region from 0 ($k_z z_0 = 0$) to 9.2 cm^{-1} ($k_z z_0 = \pi/2$). With increasing magnetic field after passing 1.5 T, the slow cyclotron mode moves to the right, and points 1 and 2 merge and disappear. The slow cyclotron mode becomes coupled to the EH_{01} mode only at point 3,

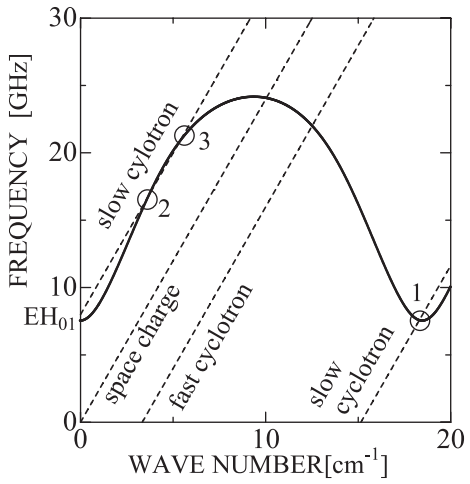

Fig. 9 Dispersion curve of EH_{01} mode. Three beam lines of the space charge, fast cyclotron, and slow cyclotron modes are plotted for $B_0 = 1.5$ T.

leading to a discontinuity in the growth rate near 1.5 T. In summary, the slow cyclotron mode couples to the EH_{01} mode in the backward regions of −1.5 T and 1.8-2.0 T. At 1.5-1.8 T, the slow instability occurs in the forward region.

4. Conclusion

We develop a numerical code for a sinusoidally corrugated waveguide with a finitely thick annular beam considering three-dimensional beam perturbations. The self-consistent field analysis is improved for an oversized SWS, and the slow cyclotron and Cherenkov instabilities are numerically examined. Nonaxisymmetric instabilities are excited even in a completely axisymmetric system. The growth rates are almost the same in nonaxisymmetric instabilities with $m = \pm 1$ and axisymmetric instabilities. The slow cyclotron and Cherenkov instabilities depend on the annular thickness. The Cherenkov instability has a weak dependence on the guiding magnetic field, while the slow cyclotron instability depends strongly on the magnetic field. Our numerical code can analyze the dependence of slow-wave instabilities and will play an important role in numerical analyses of weakly relativistic oversized BWO and slow cyclotron maser experiments.

Acknowledgments

This work was partially supported by the Grant-in-Aid for Scientific Research from the Japan Society for the Promotion of Science and by the NIFS Collaboration Research Program.

[1] K. Ogura *et al.*, IEEJ Trans. FM. **125**, 733 (2005).
[2] Y. Takamura *et al.*, Plasma Fusion Res. **3**, S1078 (2008).
[3] S. Aoyama *et al.*, Trans. Fusion Sci. Tech. **51**, 325 (2007).
[4] J. R. Pierce, *Traveling-Wave Tube* (Van Nostrand, Toronto, 1950).
[5] O. Watanabe *et al.*, Phys. Rev. E. **63**, 056503 (2001).
[6] K. Ogura *et al.*, Jpn. J. Appl. Phys. **42**, 7095 (2003).
[7] K. Ogura *et al.*, J. Plasma Phys. **72**, 905 (2006).
[8] S. Tamura *et al.*, Plasma Fusion Res. **3**, S1020 (2008).
[9] Y. Kiuchi *et al.*, Trans. Fusion Sci. Tech. **51**, 331 (2007).
[10] B. Maraghechi *et al.*, Phys. Plasmas **6**, 3778 (1999).
[11] S. Liu *et al.*, J. App. Phys. **101**, 053309 (2007).
[12] H. Yamazaki *et al.*, J. Plasma Phys. **72**, 915 (2006).